Available online at www.sciencedirect.com
ScienceDirect
Physica D 237 (2008) 339–350
PHYSICA D
www.elsevier.com/locate/physd

Lyapunov–Schmidt reduction algorithm for three-dimensional discrete vortices

Mike Lukas[a], Dmitry Pelinovsky[a,*], P.G. Kevrekidis[b]

[a] *Department of Mathematics, McMaster University, Hamilton, Ontario, Canada, L8S 4K1*
[b] *Department of Mathematics and Statistics, University of Massachusetts, Amherst, MA 01003, United States*

Received 20 December 2006; received in revised form 20 August 2007; accepted 5 September 2007
Available online 12 September 2007

Communicated by J. Lega

Abstract

We address the persistence and stability of three-dimensional vortex configurations in the discrete nonlinear Schrödinger equation and develop a symbolic package based on Wolfram's MATHEMATICA for computations of the Lyapunov–Schmidt reduction method. The Lyapunov–Schmidt reduction method is a theoretical tool which enables us to study continuations and terminations of the discrete vortices for small coupling between lattice nodes as well as the spectral stability of the persistent configurations. The method was developed earlier in the context of the two-dimensional lattice and applied to the onsite and offsite configurations (called the vortex cross and the vortex cell) by using semianalytical computations [D.E. Pelinovsky, P.G. Kevrekidis, D. Frantzeskakis, Physica D 212 (2005) 20–53; P.G. Kevrekidis, D.E. Pelinovsky, Proc. R. Soc. A 462 (2006) 2671–2694]. The present treatment develops a full symbolic computational package which takes a desired waveform at the anticontinuum limit of uncoupled sites, performs a required number of Lyapunov–Schmidt reductions and outputs the predictions on whether the configuration persists, for finite coupling, in the three-dimensional lattice and whether it is stable or unstable. It also provides approximations for the eigenvalues of the linearized stability problem. We report a number of applications of the algorithm to important multisite three-dimensional configurations, such as the simple cube, the double cross and the diamond. For each configuration, we identify exactly one solution, which is stable for small coupling between lattice nodes.

Keywords: Discrete nonlinear Schrödinger equation; Discrete vortices; Existence and stability; Lyapunov–Schmidt reductions; Symbolic computations

1. Introduction

Over the last decade, nonlinear dynamic lattices and the coherent structures that arise in them have attracted considerable attention. This can be mainly attributed to a diverse set of research themes where the corresponding mathematical models have emerged as an appropriate description of the physical problem. Such areas include, but are not limited to, arrays of nonlinear optical waveguides [1] and photorefractive crystal lattices [2], Bose–Einstein condensates (BECs) trapped in optical lattices [3], Josephson-junction ladders [4], micromechanical models of cantilever arrays [5] and simple models of the complex dynamics of the DNA double strand [6]. These, in turn, have spurted an increasing mathematical interest in Hamiltonian discrete systems and produced a considerable volume of theoretical results, which have partially been summarized in the reviews [7].

Arguably, the most prototypical among the discrete nonlinear Hamiltonian models is the discrete, nonlinear Schrödinger equation (DNLS) [8], which results from a centred-difference discretization of its continuum analogue, the nonlinear Schrödinger equation [9]. The DNLS model arises most notably in the nonlinear optics of waveguide arrays, where it was developed as an envelope wave description of the electric field in each of the waveguides [10]. It was also systematically derived as a tight-binding model for BECs trapped in optical lattices [11]. In other settings, such as e.g. photorefractive crystals, the validity of the DNLS model

* Corresponding author.
E-mail address: dmpeli@math.mcmaster.ca (D. Pelinovsky).

0167-2789/$ - see front matter
doi:10.1016/j.physd.2007.09.005

is more limited, yet still a lot of its qualitative features can be observed even experimentally. It is for this reason that this simple yet rich model has been used to justify numerous experimental observations in the above-mentioned areas, including the formation of discrete solitons [12], the existence of Peierls–Nabarro barriers for such waves [13], the modulational instability of uniform states both in optical [14] and in BEC [15] experiments, and the formation of discrete two-dimensional vortices [16], among many others. In the earlier work of [17] and [18], we studied systematically the solutions that can be obtained in the one- and two-dimensional DNLS model respectively, using a combination of methods of Lyapunov–Schmidt reductions and perturbation theory in the, so-called, anti-continuum limit of lattice sites uncoupled with each other.

In the present paper, we provide a mathematical framework and a symbolic package for the systematic computations of the existence and the stability of localized states in the fully three-dimensional DNLS model. To the best of our knowledge, this is the first time that systematic stability results have been developed for the three-dimensional system. Earlier numerical work in [19] revealed a considerable wealth of possible states, including octupoles, diamonds and vortex cubes, among many others. It is these states and different variants thereof that our systematic methodology addresses in the present publication, by formulating a symbolic approach that can be straightforwardly used to study the persistence and spectral stability of *any* desired configuration.

Our results on the three-dimensional DNLS model cannot be applied to dynamics of waveguide arrays since the third spatial direction in the optical problem represents the evolution variable. However, the model is still relevant to BECs and an additional possibility for its physical realization is offered by a three-dimensional crystal built of microresonators [20].

Our article is organized as follows. Section 2 formulates the mathematical problem of interest. Section 3 presents the main results for the development of the computational algorithm based on the Lyapunov–Schmidt reduction method. Section 4 reports the application of the computational algorithm to three kinds of three-dimensional vortex configurations. Section 5 compares these results with direct numerical bifurcation results of the three-dimensional DNLS model. Section 6 concludes the paper.

2. Formulation of the problem

We consider the discrete three-dimensional nonlinear Schrödinger (DNLS) model in the form

$$\mathrm{i}\dot{u}_n + \epsilon\Delta u_n + |u_n|^2 u_n = 0, \quad n \in \mathbb{Z}^3,\ t \in \mathbb{R}_+,\ u_n \in \mathbb{C}, \tag{2.1}$$

where $\epsilon > 0$ is the coupling strength (which can also be thought of as the reciprocal squared, lattice spacing) and Δu_n is the discrete, three-dimensional Laplacian

$$\Delta u_n = u_{n+e_1} + u_{n-e_1} + u_{n+e_2} + u_{n-e_2} + u_{n+e_3} + u_{n-e_3} - 6u_n, \quad n \in \mathbb{Z}^3,$$

with $\{e_1, e_2, e_3\}$ being standard unit vectors in $\mathbb{Z}^3$. The DNLS equation (2.1) is a Hamiltonian system with the Hamiltonian function

$$H = \epsilon\left(\|u_{n+e_1} - u_n\|^2_{l^2(\mathbb{Z}^3)} + \|u_{n+e_2} - u_n\|^2_{l^2(\mathbb{Z}^3)} + \|u_{n+e_3} - u_n\|^2_{l^2(\mathbb{Z}^3)}\right) - \frac{1}{2}\|u_n\|^4_{l^4(\mathbb{Z}^3)}, \tag{2.2}$$

which is referred to as the energy of the discrete system. Due to invariance of the DNLS equation (2.1) with respect to time translation $u_n(t) \mapsto u_n(t - t_0)$, $\forall t_0 \in \mathbb{R}$, the energy H is constant in time, such that $H(t) = H(0)$. Another conserved quantity is the discrete l^2-norm $Q = \|u_n(t)\|^2_{l^2(\mathbb{Z}^3)}$, such that $Q(t) = Q(0)$, which is related to the invariance of the DNLS equation (2.1) with respect to the gauge transformation $u_n(t) \mapsto u_n(t)\mathrm{e}^{\mathrm{i}\theta_0}$, $\forall\theta_0 \in \mathbb{R}$.

Let $\mathbf{u}$ be a vector for the triple-indexed, doubly-infinite, two-component sequences of real and imaginary parts of $\{u_n\}_{n\in\mathbb{Z}^3}$, such that the 2-block at the node $n \in \mathbb{Z}^3$ is

$$\mathbf{u}_n = \begin{bmatrix} \mathrm{Re}(u_n) \\ \mathrm{Im}(u_n) \end{bmatrix}.$$

The natural phase space of the DNLS equation (2.1) is $X = l^2_s(\mathbb{Z}^3)$ for $s > \frac{3}{2}$ with the squared norm

$$\|\mathbf{u}\|^2 = \sum_{n\in\mathbb{Z}^3} (1 + |n|^2)^s |u_n|^2.$$

Because $l^2_s(\mathbb{Z}^3)$ forms a Banach algebra for $s > \frac{3}{2}$, both H and Q are bounded and the vector field of the DNLS equation (2.1) is closed if $\mathbf{u} \in l^2_s(\mathbb{Z}^3)$ with $s > \frac{3}{2}$. The DNLS equation (2.1) can be cast as a dynamic system $\frac{\mathrm{d}\mathbf{u}}{\mathrm{d}t} = J\nabla H[\mathbf{u}]$, where $H[\mathbf{u}] : X \mapsto \mathbb{R}$ is the Hamiltonian function (2.2) and (J, ∇) are the standard symplectic and gradient operators. Operators (J, ∇) are block-diagonal with the 2-block at the node $n \in \mathbb{Z}^3$ being

$$J_n = \begin{bmatrix} 0 & 1 \\ -1 & 0 \end{bmatrix}, \qquad \nabla_n = \begin{bmatrix} \partial_{\mathrm{Re}(u_n)} \\ \partial_{\mathrm{Im}(u_n)} \end{bmatrix}.$$

We consider the time-periodic (stationary) solutions of the DNLS equation (2.1) in the form

$$u_n(t) = \phi_n \mathrm{e}^{\mathrm{i}(1-6\epsilon)t}, \quad n \in \mathbb{Z}^3,\ \phi_n \in \mathbb{C}, \tag{2.3}$$

where all parameters have been normalized for convenience. The sequence $\{\phi_n\}_{n\in\mathbb{Z}^3}$ is a solution of the difference equation

$$(1 - |\phi_n|^2)\phi_n = \epsilon\Sigma\phi_n, \quad \Sigma = \Delta + 6,\ n \in \mathbb{Z}^3. \tag{2.4}$$

The stationary equation (2.4) can be obtained by variation of the Lyapunov functional $\Lambda[\mathbf{u}] = H[\mathbf{u}] + (1 - 6\epsilon)Q[\mathbf{u}]$, such that the Euler–Lagrange equation $\nabla\Lambda[\mathbf{u}]|_{\mathbf{u}=\boldsymbol{\phi}} = 0$ results in Eq. (2.4).

If the localized solution $\boldsymbol{\phi}$ of the difference equation (2.4) exists, the time-evolution of the DNLS equation (2.1) near the time-periodic space-localized solution (2.3) is defined by the linearization

$$u_n(t) = \mathrm{e}^{\mathrm{i}(1-6\epsilon)t}\left(\phi_n + a_n\mathrm{e}^{\lambda t} + \bar{b}_n\mathrm{e}^{\bar{\lambda}t}\right), \quad n \in \mathbb{Z}^3, \tag{2.5}$$

where λ is the spectral parameter and the sequence $\{(a_n, b_n)\}_{n\in\mathbb{Z}^3}$ solves the linear eigenvalue problem for difference operators

$$\left(1-2|\phi_n|^2\right)a_n - \phi_n^2 b_n - \epsilon\Sigma a_n = \mathrm{i}\lambda a_n,$$
$$-\bar{\phi}_n^2 a_n + \left(1-2|\phi_n|^2\right)b_n - \epsilon\Sigma b_n = -\mathrm{i}\lambda b_n, \quad n\in\mathbb{Z}^3. \quad (2.6)$$

If there exists a solution with $\mathrm{Re}(\lambda) > 0$, the stationary solution (2.3) is called *spectrally unstable*. Otherwise, it is neutrally spectrally stable.

The difference equation (2.4) with $\epsilon = 0$ has a general set of localized modes on $n\in\mathbb{Z}^3$:

$$\phi_n^{(0)} = \begin{cases} \mathrm{e}^{\mathrm{i}\theta_n}, & n\in S, \\ 0, & n\in S^\perp, \end{cases} \quad (2.7)$$

where S is a bounded set of nodes on the lattice $n\in\mathbb{Z}^3$, $S^\perp = \mathbb{Z}^3\setminus S$, and $\{\theta_n\}_{n\in S}$ is a set of phase configurations. The set $\{\theta_n\}_{n\in S}$ is arbitrary for $\epsilon = 0$. It is called a *vortex configuration* if $\theta_{n_0} = 0$ for an arbitrary chosen node $n_0\in S\subset\mathbb{Z}^3$ and $\theta_{n_1}\neq\{0,\pi\}$ for at least one $n_1\in S$, $n_1\neq n_0$. If $\theta_n\in\{0,\pi\}$, $\forall n\in S$, it is dubbed a *discrete soliton*. We address here the main question: *For what vortex configurations, the localized mode (2.7) can be continued in the difference equation (2.4) for small $\epsilon > 0$ and is spectrally stable in the linear eigenvalue problem (2.6)*?

Although the question will be answered with a general algorithm, we would like to consider specific vortex configurations in the three-dimensional DNLS equation. Some of these configurations have appeared in the previous works [19] as they are thought to be elementary building blocks of three-dimensional discrete localized structures. The three specific configurations are formulated in terms of the limiting solution (2.7).

(i) *A simple cube* consists of two adjacent planes of aligned vortex cells. More precisely, we set $S = S_0\oplus S_1$, where

$$S_l = \{(0,0,l),(1,0,l),(1,1,l),(0,1,l)\}, \quad l = 0,1, \quad (2.8)$$

such that $N = \dim(S) = 8$. Let j be the index enumerating nodes in the contours S_0 and S_1 according to the order (2.8). Let $\theta_{l,j}$ be the corresponding phase in the set $\{\theta_n\}_{n\in S}$, where $l = 0,1$ and $j = 1,2,3,4$. Then, the simple cube vortex configurations are

$$\theta_{0,j} = \frac{\pi(j-1)}{2}, \qquad \theta_{1,j} = \theta_0 + s_0\frac{\pi(j-1)}{2}, \quad j = 1,2,3,4, \quad (2.9)$$

where $\theta_0 = \{0,\frac{\pi}{2},\pi,\frac{3\pi}{2}\}$ and $s_0 = \{+1,-1\}$. Two configurations with $s_0 = -1$ are redundant: the cases $\theta_0 = \pi$ and $\theta_0 = \frac{3\pi}{2}$ can be obtained from the cases $\theta_0 = 0$ and $\theta_0 = \frac{\pi}{2}$ respectively by multiplication of u_n by i and rotation of the whole structure by 90°. In what follows, we only consider the six irreducible vortex configurations and show that only three configurations persist for $\epsilon\neq 0$ and only one configuration with $\theta_0 = \pi$ and $s_0 = 1$ is spectrally stable.

(ii) *A double cross* consists of two symmetric planes of aligned vortex crosses separated by an empty plane. More precisely, we set $S = S_{-1}\oplus S_1$, where

$$S_l = \{(-1,0,l),(0,-1,l),(1,0,l),(0,1,l)\}, \quad l = -1,1, \quad (2.10)$$

such that $N = \dim(S) = 8$. By using the same convention as in (i), the double cross vortex configurations are expressed by

$$\theta_{-1,j} = \frac{\pi(j-1)}{2}, \qquad \theta_{1,j} = \theta_0 + s_0\frac{\pi(j-1)}{2}, \quad j = 1,2,3,4, \quad (2.11)$$

where $\theta_0 = \{0,\frac{\pi}{2},\pi,\frac{3\pi}{2}\}$ and $s_0 = \{+1,-1\}$. Similarly to the simple cube vortex configurations, we will consider six irreducible vortex configurations and show that three configurations persist for $\epsilon\neq 0$ and only one configuration with $\theta_0 = \pi$ and $s_0 = 1$ is spectrally stable.

(iii) *A diamond* consists of a quadrupole in a central plane, surrounded by two symmetric central off-plane nodes. More precisely, we set $S = S_{-1}\oplus S_0\oplus S_1$, where

$$S_0 = \{(-1,0,0),(0,-1,0),(1,0,0),(0,1,0)\}, \quad S_{\pm1} = \{(0,0,\pm1)\}, \quad (2.12)$$

such that $N = \dim(S) = 6$. By using the same convention as in (i), the diamond vortex configurations are expressed by

$$\theta_{0,j} = \pi(j-1), \quad j = 1,2,3,4, \qquad \theta_{\pm1,0} = \theta_0^{\pm}, \quad (2.13)$$

where $\theta_0^{\pm} = \{0,\frac{\pi}{2},\pi,\frac{3\pi}{2}\}$. Six configurations with $\theta_0^- > \theta_0^+$ are redundant as they can be obtained from the corresponding configurations with $\theta_0^- < \theta_0^+$ by reflection: $\theta_0^{\pm}\mapsto\theta_0^{\mp}$. Three other configurations with $\theta_0^- = \theta_0^+ = \{\pi,\frac{3\pi}{2}\}$ and $\theta_0^- = \pi$, $\theta_0^+ = \frac{3\pi}{2}$ can be obtained from the configurations $\theta_0^- = \theta_0^+ = \{0,\frac{\pi}{2}\}$ and $\theta_0^- = 0$, $\theta_0^+ = \frac{\pi}{2}$ respectively by multiplication of u_n by -1 and rotation of the whole structure by 180°. One more configuration with $\theta_0^- = 0$, $\theta_0^+ = \frac{3\pi}{2}$ can be obtained from the configuration with $\theta_0^- = 0$, $\theta_0^+ = \frac{\pi}{2}$ by complex conjugation. In what follows, we only consider the six irreducible vortex configurations and show that only three configurations persist for $\epsilon\neq 0$ and only one configuration with $\theta_0^- = \frac{\pi}{2}$ and $\theta_0^+ = \frac{3\pi}{2}$ is spectrally stable.

Three characteristic representatives of each of the specified configurations (a vortex cube, a double cross and a diamond) are shown in Fig. 1. They correspond to spectrally stable solutions in the three-dimensional lattice. For all other configurations, the sets of active nodes S remain the same, yet the phases of these nodes vary.

3. Review of the Lyapunov–Schmidt reduction algorithm

We review the main results of [18], where the Lyapunov–Schmidt reduction method is developed to answer the question posed in Section 2. The main idea of the reduction method is to track the breaking of the extra symmetries, which exist in

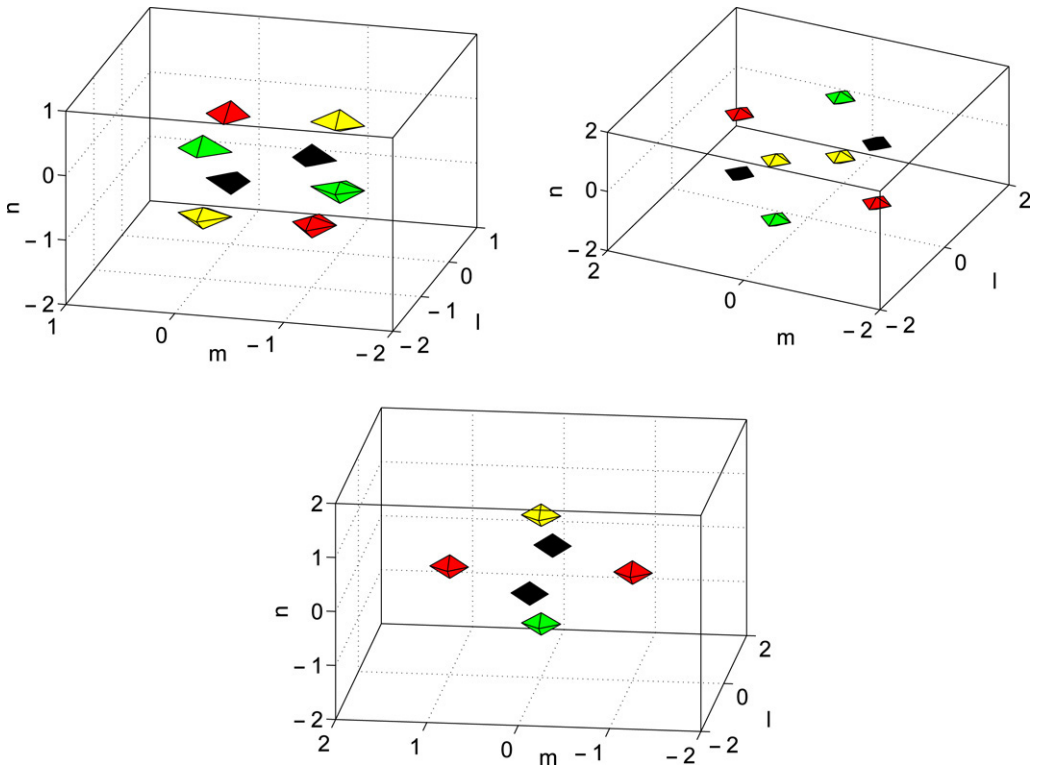

Fig. 1. Stable configurations in the three-dimensional lattice: a vortex cube (top left), a double cross (top right) and a diamond (bottom) (cf. with Figs. 4, 7 and 10). All configurations are for $\epsilon = 0.1$. The darker colours (black and red in the web version) correspond to nodes where $\mathrm{Re}\, u$ becomes 1 and -1 respectively. The lighter colours (green and yellow in the web version) correspond to nodes where $\mathrm{Im}\, u$ becomes 1 and -1 respectively.

the decoupled problem with $\epsilon = 0$. Indeed, the phases of each node in the set of active nodes S are arbitrary in the decoupled problem, whereas the phases may change only via the one-parameter gauge invariance in the coupled problem with $\epsilon \neq 0$.

Let $\mathcal{O}(0)$ be a small neighbourhood of 0 on $\mathbb{R}$ for parameter ϵ. Let $N = \dim(S)$ and $\mathcal{T}$ be the torus on $[0, 2\pi]^N$ for the vector $\boldsymbol{\theta}$ of phase components $\{\theta_n\}_{n\in S}$. The nonlinear vector field $\mathbf{F}(\boldsymbol{\phi}, \epsilon)$ on $\boldsymbol{\phi} \in X$ and $\epsilon \in \mathbb{R}$ is defined by its 2-block at the node $n \in \mathbb{Z}$ in the form

$$\mathbf{F}_n(\boldsymbol{\phi}, \epsilon) = \begin{bmatrix} (1 - |\phi_n|^2)\phi_n - \epsilon \Sigma \phi_n \\ (1 - |\phi_n|^2)\bar{\phi}_n - \epsilon \Sigma \bar{\phi}_n \end{bmatrix}. \tag{3.1}$$

The Jacobian $D_{\boldsymbol{\phi}}\mathbf{F}(\boldsymbol{\phi}, \epsilon)$ of the nonlinear-vector field $\mathbf{F}(\boldsymbol{\phi}, \epsilon)$ at the solution $\boldsymbol{\phi}$ for any $\epsilon \in \mathbb{R}$ coincides with the *linearized energy operator* $\mathcal{H}$, which defines the quadratic form for the Lyapunov function $\Lambda[\mathbf{u}] = H[\mathbf{u}] + (1 - 6\epsilon)Q[\mathbf{u}]$ in the form

$$\Lambda[\mathbf{u}] = \Lambda[\boldsymbol{\phi}] + \frac{1}{2}(\boldsymbol{\psi}, \mathcal{H}\boldsymbol{\psi}) + \mathrm{O}(\|\boldsymbol{\psi}\|^3),$$

where the 2-block of $\boldsymbol{\psi}$ is defined at the node $n \in \mathbb{Z}^3$ by

$$\boldsymbol{\psi}_n = \begin{bmatrix} a_n \\ b_n \end{bmatrix}.$$

The matrix operator $\mathcal{H}$ on $\boldsymbol{\psi}$ is not block-diagonal due to the presence of the shift operator Σ. We can still use a formal notation $\mathcal{H}_n$ for the "2-block" of $\mathcal{H}$ at the node $n \in \mathbb{Z}^3$

$$\mathcal{H}_n = \begin{pmatrix} 1 - 2|\phi_n|^2 & -\phi_n^2 \\ -\bar{\phi}_n^2 & 1 - 2|\phi_n|^2 \end{pmatrix} - \epsilon \left(s_{+e_1} + s_{-e_1} + s_{+e_2} + s_{-e_2} + s_{+e_3} + s_{-e_3}\right) \begin{pmatrix} 1 & 0 \\ 0 & 1 \end{pmatrix}, \tag{3.2}$$

where $s_{\pm e_j} u_n = u_{n\pm e_j}$ for $j = 1, 2, 3$. This notation allows us to write the matrix-vector form $\mathcal{H}\boldsymbol{\psi}$ in the component form $\mathcal{H}_n\boldsymbol{\psi}_n$ at each node $n \in \mathbb{Z}^3$. In particular, the linear eigenvalue problem (2.6) can be rewritten in the matrix-vector form

$$\sigma\mathcal{H}\boldsymbol{\psi} = \mathrm{i}\lambda\boldsymbol{\psi}, \tag{3.3}$$

where $\boldsymbol{\psi} \in X$ and the 2-block of σ is a diagonal matrix of $(1, -1)$ at each node $n \in \mathbb{Z}^3$. It should be noted here that the eigenvector $\boldsymbol{\psi}$ of the linear eigenvalue problem (3.3) has elements $b_n = \bar{a}_n$ for all $n \in \mathbb{Z}^3$ only if $\lambda = \bar{\lambda}$. For complex eigenvalues λ, the elements b_n and a_n are extended in the complex domain with $b_n \neq \bar{a}_n$.

Let $\boldsymbol{\phi}^{(0)} = \boldsymbol{\phi}^{(0)}(\boldsymbol{\theta})$ be the solution (2.7). By explicit computations, $\mathbf{F}(\boldsymbol{\phi}^{(0)}, 0) = \mathbf{0}$ is satisfied and $\mathcal{H}^{(0)} = D_{\boldsymbol{\phi}}\mathbf{F}(\boldsymbol{\phi}^{(0)}, 0)$ is block-diagonal with the 2-block at the node $n \in \mathbb{Z}^3$ given by

$$(\mathcal{H}^{(0)})_n = \begin{bmatrix} 1 & 0 \\ 0 & 1 \end{bmatrix}, \quad n \in S^{\perp},$$

$$(\mathcal{H}^{(0)})_n = \begin{bmatrix} -1 & -\mathrm{e}^{2\mathrm{i}\theta_n} \\ -\mathrm{e}^{-2\mathrm{i}\theta_n} & -1 \end{bmatrix}, \quad n \in S.$$

We note that $\mathcal{H}^{(0)}\mathbf{e}_n = \mathbf{0}$ and $\mathcal{H}^{(0)}\hat{\mathbf{e}}_n = -2\hat{\mathbf{e}}_n$, $n \in S \subset \mathbb{Z}^3$, where the 2-blocks of eigenvectors $\mathbf{e}_n$ and $\hat{\mathbf{e}}_n$ at the node $k \in \mathbb{Z}^3$

are given by

$$(\mathbf{e}_n)_k = \mathrm{i}\begin{bmatrix} \mathrm{e}^{\mathrm{i}\theta_n} \\ -\mathrm{e}^{-\mathrm{i}\theta_n} \end{bmatrix} \quad \delta_{k,n}, \qquad (\hat{\mathbf{e}}_n)_k = \begin{bmatrix} \mathrm{e}^{\mathrm{i}\theta_n} \\ \mathrm{e}^{-\mathrm{i}\theta_n} \end{bmatrix} \quad \delta_{k,n},$$

with $\delta_{k,n}$ being a standard Kroneker symbol. Therefore, $\mathrm{Ker}(\mathcal{H}^{(0)}) = \mathrm{Span}(\{\mathbf{e}_n\}_{n\in S}) \subset X$. Let $\mathcal{P} : X \mapsto \mathrm{Ker}(\mathcal{H}^{(0)})$ be an orthogonal projection operator to the N-dimensional kernel of $\mathcal{H}^{(0)}$. In the explicit form, the projection operator $\mathcal{P}$ is expressed by

$$\forall \mathbf{f} \in X : \quad (\mathcal{P}\mathbf{f})_n = \frac{1}{2\mathrm{i}}\left(\mathrm{e}^{-\mathrm{i}\theta_n}(\mathbf{f})_n - \mathrm{e}^{\mathrm{i}\theta_n}(\bar{\mathbf{f}})_n\right) \quad n \in S. \tag{3.4}$$

Since the operator $\mathcal{H}^{(0)}$ is a self-adjoint Fredholm operator of zero index, the decomposition $X = \mathrm{Ker}(\mathcal{H}^{(0)}) \oplus \mathrm{Range}(\mathcal{H}^{(0)})$ is well defined and so is the projection operator $(\mathcal{I} - \mathcal{P}) : X \mapsto \mathrm{Range}(\mathcal{H}^{(0)})$. By using the Lyapunov–Schmidt reduction algorithm, we consider the decomposition

$$\boldsymbol{\phi} = \boldsymbol{\phi}^{(0)}(\boldsymbol{\theta}) + \sum_{n\in S} \alpha_n \mathbf{e}_n + \boldsymbol{\varphi} \in X, \tag{3.5}$$

where $\boldsymbol{\varphi} \in \mathrm{Range}(\mathcal{H}^{(0)})$ and $\alpha_n \in \mathbb{R}$ for each $n \in S$. We note that

$$\forall \boldsymbol{\theta}_0 \in \mathcal{T} : \quad \boldsymbol{\phi}^{(0)}(\boldsymbol{\theta}_0) + \sum_{n\in S} \alpha_n \mathbf{e}_n = \boldsymbol{\phi}^{(0)}(\boldsymbol{\theta}_0 + \boldsymbol{\alpha}) + \mathrm{O}(\|\boldsymbol{\alpha}\|^2_{\mathbb{R}^n}). \tag{3.6}$$

Since the values of $\boldsymbol{\theta}$ in $\boldsymbol{\phi}^{(0)}(\boldsymbol{\theta})$ have not been defined yet, we can set $\alpha_n = 0$, $n \in S$ without loss of generality. The splitting equations in the Lyapunov–Schmidt reduction algorithm are

$$\mathcal{P}\mathbf{F}(\boldsymbol{\phi}^{(0)}(\boldsymbol{\theta}) + \boldsymbol{\varphi}, \epsilon) = 0, \qquad (\mathcal{I} - \mathcal{P})\mathbf{F}(\boldsymbol{\phi}^{(0)}(\boldsymbol{\theta}) + \boldsymbol{\varphi}, \epsilon) = 0.$$

We note that $(\mathcal{I}-\mathcal{P})\mathcal{H}(\mathcal{I}-\mathcal{P}) : \mathrm{Range}(\mathcal{H}^{(0)}) \mapsto \mathrm{Range}(\mathcal{H}^{(0)})$ is analytic in $\epsilon \in \mathcal{O}(0)$ and invertible at $\epsilon = 0$, while $\mathbf{F}(\boldsymbol{\phi}, \epsilon)$ is analytic in $\epsilon \in \mathcal{O}(0)$. By the Implicit Function Theorem for Analytic Vector Fields, there exists a unique solution $\boldsymbol{\varphi} \in X$ analytic in $\epsilon \in \mathcal{O}(0)$ and dependent on $\boldsymbol{\theta} \in \mathcal{T}$, such that $\boldsymbol{\varphi} \equiv \boldsymbol{\varphi}(\boldsymbol{\theta}, \epsilon)$ and $\|\boldsymbol{\varphi}\|_X = \mathrm{O}(\epsilon)$ as $\epsilon \to 0$. As a result, there exists the nonlinear vector field $\mathbf{g} : \mathcal{T} \times \mathbb{R} \mapsto \mathbb{R}^N$, such that the Lyapunov–Schmidt bifurcation equations are

$$\mathbf{g}(\boldsymbol{\theta}, \epsilon) = \mathcal{P}\mathbf{F}(\boldsymbol{\phi}^{(0)}(\boldsymbol{\theta}) + \boldsymbol{\varphi}(\boldsymbol{\theta}, \epsilon), \epsilon) = 0. \tag{3.7}$$

By the construction, the function $\mathbf{g}(\boldsymbol{\theta}, \epsilon)$ is analytic in $\epsilon \in \mathcal{O}(0)$ and $\mathbf{g}(\boldsymbol{\theta}, 0) = \mathbf{0}$ for any $\boldsymbol{\theta} \in \mathcal{T}$. Therefore, $\mathbf{g}(\boldsymbol{\theta}, \epsilon)$ can be represented for $\epsilon \in \mathrm{O}(0)$ by the Taylor series

$$\mathbf{g}(\boldsymbol{\theta}, \epsilon) = \sum_{k=1}^{\infty} \epsilon^k \mathbf{g}^{(k)}(\boldsymbol{\theta}). \tag{3.8}$$

By the gauge symmetry, the function $\mathbf{g}(\boldsymbol{\theta}, \epsilon)$ satisfies the following relation:

$$\forall \alpha_0 \in \mathbb{R}, \quad \forall \boldsymbol{\theta} \in \mathcal{T} : \quad \mathbf{g}(\boldsymbol{\theta} + \alpha_0 \mathbf{p}_0, \epsilon) = \mathbf{g}(\boldsymbol{\theta}, \epsilon), \tag{3.9}$$

where $\mathbf{p}_0 = (1, 1, \ldots, 1)^T \in \mathbb{R}^N$. The Lyapunov–Schmidt decomposition is summarized in the following theorem.

Theorem 1 (*Persistence*). *The limiting configuration (2.7) for $\boldsymbol{\phi}^{(0)}(\boldsymbol{\theta})$ can be continued to the domain $\epsilon \in \mathcal{O}(0)$ if and only if there exists a root $\boldsymbol{\theta}_* \in \mathcal{T}$ of the vector field $\mathbf{g}(\boldsymbol{\theta}, \epsilon)$. Moreover, if the root $\boldsymbol{\theta}_*$ is analytic in $\epsilon \in \mathcal{O}(0)$ and $\boldsymbol{\theta}_* = \boldsymbol{\theta}_0 + \mathrm{O}(\epsilon)$, the solution $\boldsymbol{\phi}$ of the difference equation (2.4) is analytic in $\epsilon \in \mathcal{O}(0)$, such that*

$$\boldsymbol{\phi} = \boldsymbol{\phi}^{(0)}(\boldsymbol{\theta}_*) + \boldsymbol{\varphi}(\boldsymbol{\theta}_*, \epsilon) = \boldsymbol{\phi}^{(0)}(\boldsymbol{\theta}_0) + \sum_{k=1}^{\infty} \epsilon^k \boldsymbol{\phi}^{(k)}(\boldsymbol{\theta}_0), \tag{3.10}$$

where $\boldsymbol{\phi}^{(k)}(\boldsymbol{\theta}_0)$, $k \in \mathbb{N}$ are independent on ϵ.

Implementation of the Lyapunov–Schmidt decomposition is based on the analysis of the convergent Taylor series expansions (3.8) and (3.10). Let $\mathcal{M} = D_{\boldsymbol{\theta}}\mathbf{g}(\boldsymbol{\theta}, \epsilon) : \mathbb{R}^N \mapsto \mathbb{R}^N$ be the Jacobian matrix evaluated at the vector $\boldsymbol{\theta} \in \mathcal{T}$. By the symmetry of the shift operators Σ, the matrix $\mathcal{M}$ is symmetric. By the gauge transformation (3.9), $\mathcal{M}\mathbf{p}_0 = \mathbf{0} \in \mathbb{R}^N$, such that the spectrum of $\mathcal{M}$ includes a zero eigenvalue. If the zero eigenvalue of $\mathcal{M}$ is simple, zeros $\boldsymbol{\theta}_*$ of the function $\mathbf{g}(\boldsymbol{\theta}, \epsilon)$ are uniquely continued in ϵ modulo the gauge transformation (3.9) by using the Implicit Function Theorem for Analytic Vector Fields.

Algorithm 1 (*Persistence*). Suppose that $\mathbf{g}^{(k)}(\boldsymbol{\theta}) \equiv \mathbf{0}$ for $k = 1, 2, \ldots, \kappa - 1$ and $\mathbf{g}^{(\kappa)}(\boldsymbol{\theta}) \neq \mathbf{0}$ for $\kappa \geq 1$. Let $\boldsymbol{\theta}_0$ be the root of $\mathbf{g}^{(\kappa)}(\boldsymbol{\theta})$ and $\mathcal{M}^{(k)} = D_{\boldsymbol{\theta}}\mathbf{g}^{(k)}(\boldsymbol{\theta}_0)$ for $k \geq \kappa$.

1. If $\mathrm{Ker}(\mathcal{M}^{(\kappa)}) = \mathrm{Span}(\mathbf{p}_0) \subset \mathbb{R}^N$, then the configuration (2.7) is uniquely continued in $\epsilon \in \mathcal{O}(0)$ modulo the gauge transformation (3.9).
2. Let $\mathrm{Ker}(\mathcal{M}^{(\kappa)}) = \mathrm{Span}(\mathbf{p}_0, \mathbf{p}_1, \ldots, \mathbf{p}_{d_\kappa}) \subset \mathbb{R}^N$ with $1 \leq d_\kappa \leq N - 1$ and $P^{(\kappa)} : \mathbb{R}^N \mapsto \mathrm{Ker}(\mathcal{M}^{(\kappa)})$ be the projection matrix. Then,
   (a) If $\mathbf{g}^{(\kappa+1)}(\boldsymbol{\theta}_0) \notin \mathrm{Range}(\mathcal{M}^{(\kappa)})$, the configuration (2.7) does not persist for any $\epsilon \neq 0$.
   (b) If $\mathbf{g}^{(\kappa+1)}(\boldsymbol{\theta}_0) \in \mathrm{Range}(\mathcal{M}^{(\kappa)})$, the configuration (2.7) is continued to the next order. Replace
   $\mathcal{M}^{(\kappa)} \mapsto P^{(\kappa)}\mathcal{M}^{(\kappa+1)}P^{(\kappa)}$,
   $P^{(\kappa)} \mapsto P^{(\kappa+1)} : \mathbb{R}^N \mapsto \mathrm{Ker}(P^{(\kappa)}\mathcal{M}^{(\kappa+1)}P^{(\kappa)})$,
   $\boldsymbol{\theta}_0 \mapsto \boldsymbol{\theta}_0 - \epsilon\left(\mathcal{M}^{(\kappa)}\right)^{-1}\mathbf{g}^{(\kappa+1)}(\boldsymbol{\theta}_0)$,
   $\mathbf{g}^{(k+1)} \mapsto \mathbf{g}^{(k+2)}$
   and repeat the previous two steps.

If the algorithm stops at the order K with $\kappa \leq K < \infty$, conclude whether the vortex configuration continues in ϵ or terminates at $\epsilon = 0$. If no $K < \infty$ exists, the algorithm does not converge in a finite number of iterations.

We should add some remarks about Algorithm 1. For subsequent iterations of the algorithm, we need to extend the power series

$$\boldsymbol{\theta}_* = \boldsymbol{\theta}_0 - \epsilon\left(\mathcal{M}^{(\kappa)}\right)^{-1}\mathbf{g}^{(\kappa+1)}(\boldsymbol{\theta}_0) + \mathrm{O}(\epsilon^2) \tag{3.11}$$

to higher orders of ϵ. This expansion is evaluated from the Taylor series (3.8). Additionally, if the algorithm does not converge in a finite number of iterations, then the particular

vortex configuration may persist beyond all orders of ϵ and have additional parameters besides the parameter α_0 in the gauge transformation (3.9).

If the algorithm converges in a finite number of iterations, it provides a binary answer on whether the configuration persists beyond $\epsilon \neq 0$ or terminates at $\epsilon = 0$. Simultaneously, the method enables us to predict spectral stability of the persistent vortex configurations. To consider stability of vortex configurations, we need to consider the spectrum of operators $\mathcal{H}$ and $\sigma\mathcal{H}$ in the neighbourhood of the zero eigenvalue for $\epsilon \in \mathcal{O}(0)$.

Using the representation (3.2) and the Taylor series expansion (3.10), we represent operator $\mathcal{H}$ by its Taylor series

$$\mathcal{H} = \mathcal{H}^{(0)} + \sum_{k=1}^{\infty} \epsilon^k \mathcal{H}^{(k)} \tag{3.12}$$

and consider the truncated eigenvalue problem for the spectrum of $\mathcal{H}$:

$$\left[\mathcal{H}^{(0)} + \epsilon\mathcal{H}^{(1)} + \cdots + \epsilon^{k-1}\mathcal{H}^{(k-1)} + \epsilon^k \mathcal{H}^{(k)} + \mathrm{O}(\epsilon^{k+1})\right]\boldsymbol{\psi} = \mu\boldsymbol{\psi},$$

where μ is eigenvalue and $\boldsymbol{\psi} \in X$ is an eigenvector.

Let us assume that Algorithm 1 produces multidimensional kernels of matrices $\mathcal{M}^{(\kappa)}$, $\mathcal{M}^{(\kappa+1)}, \ldots, \mathcal{M}^{(k-1)}$, such that $\dim\mathrm{Ker}\mathcal{M}^{(k)} < \dim\mathrm{Ker}\mathcal{M}^{(k-1)}$ for some $\kappa \leq k \leq K$. Here, κ and K are the starting and termination orders of Algorithm 1, such that the kernel of $\mathcal{M}^{(K)}$ is one-dimensional. To put this discussion on a formal footing, we let $\boldsymbol{\alpha}$ be an element of $\mathrm{Ker}(\mathcal{M}^{(\kappa)}) \cap \mathrm{Ker}(\mathcal{M}^{(\kappa+1)}) \cap \cdots \cap \mathrm{Ker}(\mathcal{M}^{(k-1)}) \subset \mathbb{R}^N$, such that $\boldsymbol{\alpha} \notin \mathrm{Ker}(\mathcal{M}^{(k)})$ for some $\kappa \leq k \leq K$. It is clear that $\boldsymbol{\alpha}$ has $(d_{k-1}+1)$ arbitrary parameters, where $d_{k-1} \leq N-1$. By using the projection operator $\mathcal{P}$ in (3.4) and the relation (3.6), we obtain that

$$\boldsymbol{\alpha} = \mathcal{P}\left(\sum_{n\in S} \alpha_n \mathbf{e}_n\right), \qquad \left(\sum_{n\in S} \alpha_n \mathbf{e}_n\right) = D_{\boldsymbol{\theta}}\boldsymbol{\phi}^{(0)}(\boldsymbol{\theta}_0)\boldsymbol{\alpha},$$

where $D_{\boldsymbol{\theta}}\boldsymbol{\phi}^{(0)}(\boldsymbol{\theta}_0)$ is the Jacobian matrix of the infinite-dimensional vector $\boldsymbol{\phi}^{(0)}(\boldsymbol{\theta})$ with respect to the N-dimensional vector $\boldsymbol{\theta}$. It is clear that

$$\mathcal{H}^{(0)}\boldsymbol{\psi}^{(0)} = 0, \quad \text{where } \boldsymbol{\psi}^{(0)} = \sum_{n\in S} \alpha_n \mathbf{e}_n = D_{\boldsymbol{\theta}}\boldsymbol{\phi}^{(0)}(\boldsymbol{\theta}_0)\boldsymbol{\alpha}.$$

Moreover, the partial $(k-1)$-th sum of the power series (3.10) gives the zero of the nonlinear-vector field (3.1) up to the order $\mathrm{O}(\epsilon^k)$ and has $(d_{k-1}+1)$ arbitrary parameters if $\boldsymbol{\theta}_0$ is shifted in the direction of the vector $\boldsymbol{\alpha}$. At the tangent space of the nonlinear-vector fields (3.1) in the direction of $\boldsymbol{\alpha}$, the linear inhomogeneous system

$$\mathcal{H}^{(0)}\boldsymbol{\psi}^{(m)} + \mathcal{H}^{(1)}\boldsymbol{\psi}^{(m-1)} + \cdots + \mathcal{H}^{(m)}\boldsymbol{\psi}^{(0)} = \mathbf{0}$$

has a particular solution in the form $\boldsymbol{\psi}^{(m)} = D_{\boldsymbol{\theta}}\boldsymbol{\phi}^{(m)}(\boldsymbol{\theta}_0)\boldsymbol{\alpha}$ for $m = 1, 2, \ldots, k-1$. By extending the regular perturbation series for isolated zero eigenvalues of $\mathcal{H}^{(0)}$,

$$\begin{aligned}\boldsymbol{\psi} &= \boldsymbol{\psi}^{(0)} + \epsilon\boldsymbol{\psi}^{(1)} + \cdots + \epsilon^k\boldsymbol{\psi}^{(k)} + \mathrm{O}(\epsilon^{k+1}),\\ \mu &= \mu_k\epsilon^k + \mathrm{O}(\epsilon^{k+1}),\end{aligned} \tag{3.13}$$

we obtain the linear inhomogeneous equation

$$\mathcal{H}^{(0)}\boldsymbol{\psi}^{(k)} + \mathcal{H}^{(1)}\boldsymbol{\psi}^{(k-1)} + \cdots + \mathcal{H}^{(k)}\boldsymbol{\psi}^{(0)} = \mu_k\boldsymbol{\psi}^{(0)}.$$

Applying the projection operator $\mathcal{P}$ and recalling the definition (3.7), we find that the left-hand side of the linear equation reduces to the form

$$\begin{aligned}&\mathcal{P}\left[\mathcal{H}^{(1)}D_{\boldsymbol{\theta}}\boldsymbol{\phi}^{(k-1)}(\boldsymbol{\theta}_0) + \cdots + \mathcal{H}^{(k)}D_{\boldsymbol{\theta}}\boldsymbol{\phi}^{(0)}(\boldsymbol{\theta}_0)\right]\boldsymbol{\alpha}\\ &\quad = D_{\boldsymbol{\theta}}\mathbf{g}^{(k)}(\boldsymbol{\theta}_0)\boldsymbol{\alpha} = \mathcal{M}^{(k)}\boldsymbol{\alpha},\end{aligned}$$

where we have used that $\mathcal{P}\boldsymbol{\psi}^{(0)} = \boldsymbol{\alpha}$. Therefore, μ_k is an eigenvalue of the Jacobian matrix $\mathcal{M}^{(k)}$ and $\boldsymbol{\alpha}$ is the corresponding eigenvector. The equivalence between non-zero small eigenvalues of $\mathcal{H}$ and non-zero eigenvalues of $\mathcal{M}$ is summarized in the following theorem.

Theorem 2 (*Eigenvalues of $\mathcal{H}$*). *Let Algorithm 1 converge at the K-th order and the solution $\boldsymbol{\phi}$ in Theorem 1 persist for $\epsilon \neq 0$. Then,*

$$\begin{aligned}&\lambda_{\neq 0}(\mathcal{H}) = \lambda_{\neq 0}(P^{(m-1)}\mathcal{M}^{(m)}P^{(m-1)})\epsilon^m + \mathrm{O}(\epsilon^{m+1}),\\ &\quad m = \kappa, \kappa+1, \ldots, K,\end{aligned}$$

where $\lambda_{\neq 0}(\mathcal{A})$ denotes a non-zero eigenvalue of operator $\mathcal{A}$.

Similarly to the computations of small non-zero eigenvalues of $\mathcal{H}$, we consider eigenvalues of the spectral problem (3.3) truncated at the k-th order approximation:

$$\left[\mathcal{H}^{(0)} + \epsilon\mathcal{H}^{(1)} + \cdots + \epsilon^{k-1}\mathcal{H}^{(k-1)} + \epsilon^k\mathcal{H}^{(k)} + \mathrm{O}(\epsilon^{k+1})\right]\boldsymbol{\psi} = \mathrm{i}\lambda\sigma\boldsymbol{\psi}.$$

By using relations $\hat{\mathbf{e}}_n = -\mathrm{i}\sigma\mathbf{e}_n$ and $\mathcal{H}^{(0)}\hat{\mathbf{e}}_n = -2\hat{\mathbf{e}}_n$ for all $n \in S$, we can see that the linear inhomogeneous equation

$$\mathcal{H}^{(0)}\boldsymbol{\varphi}^{(0)} = 2\mathrm{i}\sigma D_{\boldsymbol{\theta}}\boldsymbol{\phi}^{(0)}(\boldsymbol{\theta}_0)\boldsymbol{\alpha}$$

has a solution

$$\boldsymbol{\varphi}^{(0)} = \sum_{n\in S} \alpha_n\hat{\mathbf{e}}_n = \boldsymbol{\Phi}^{(0)}(\boldsymbol{\theta}_0)\boldsymbol{\alpha},$$

where $\boldsymbol{\Phi}^{(0)}(\boldsymbol{\theta}_0)$ is the matrix extension of $\boldsymbol{\phi}^{(0)}(\boldsymbol{\theta}_0)$, which consists of vector columns $\hat{\mathbf{e}}_n$, $n \in S$. Similarly, there exists a particular solution of the inhomogeneous problem

$$\begin{aligned}&\mathcal{H}^{(0)}\boldsymbol{\varphi}^{(m)} + \mathcal{H}^{(1)}\boldsymbol{\varphi}^{(m-1)} + \cdots + \mathcal{H}^{(m)}\boldsymbol{\varphi}^{(0)}\\ &\quad = 2\mathrm{i}\sigma D_{\boldsymbol{\theta}}\boldsymbol{\phi}^{(m)}(\boldsymbol{\theta}_0)\boldsymbol{\alpha}, \quad m = 1, 2, \ldots, k',\end{aligned}$$

in the form $\boldsymbol{\varphi}^{(m)} = \boldsymbol{\Phi}^{(m)}(\boldsymbol{\theta}_0)\boldsymbol{\alpha}$, where $k' = (k-1)/2$ if k is odd and $k' = k/2 - 1$ if k is even. By extending the regular perturbation series for isolated zero eigenvalue of $\sigma\mathcal{H}^{(0)}$,

$$\begin{aligned}\boldsymbol{\psi} &= \boldsymbol{\psi}^{(0)} + \epsilon\boldsymbol{\psi}^{(1)} + \cdots + \epsilon^{k-1}\boldsymbol{\psi}^{(k-1)}\\ &\quad + \frac{1}{2}\lambda\left(\boldsymbol{\varphi}^{(0)} + \epsilon\boldsymbol{\varphi}^{(1)} + \cdots + \epsilon^{k'}\boldsymbol{\varphi}^{(k')}\right)\\ &\quad + \epsilon^k\boldsymbol{\psi}^{(k)} + \mathrm{O}(\epsilon^{k+1}),\end{aligned} \tag{3.14}$$

where $\boldsymbol{\psi}^{(m)} = D_{\boldsymbol{\theta}}\boldsymbol{\phi}^{(m)}(\boldsymbol{\theta}_0)\boldsymbol{\alpha}$ for $m = 0, 1, \ldots, k-1$, $\boldsymbol{\varphi}^{(m)} = \boldsymbol{\Phi}^{(m)}(\boldsymbol{\theta}_0)\boldsymbol{\alpha}$ for $m = 0, 1, \ldots, k'$, and $\lambda = \epsilon^{k/2}\lambda_{k/2} + \mathrm{O}(\epsilon^{k/2+1})$,

we obtain a linear inhomogeneous problem for $\boldsymbol{\psi}^{(k)}$ at the order $O(\epsilon^k)$. When k is odd, the linear problem takes the form

$$\mathcal{H}^{(0)}\boldsymbol{\psi}^{(k)} + \mathcal{H}^{(1)}\boldsymbol{\psi}^{(k-1)} + \cdots + \mathcal{H}^{(k)}\boldsymbol{\psi}^{(0)} = \frac{\mathrm{i}}{2}\lambda_{k/2}^2\sigma\boldsymbol{\varphi}^{(0)}. \tag{3.15}$$

When k is even, the linear problem takes the form

$$\begin{aligned}&\mathcal{H}^{(0)}\boldsymbol{\psi}^{(k)} + \mathcal{H}^{(1)}\boldsymbol{\psi}^{(k-1)} + \cdots + \mathcal{H}^{(k)}\boldsymbol{\psi}^{(0)}\\ &\quad + \frac{1}{2}\lambda_{k/2}\left(\mathcal{H}^{(1)}\boldsymbol{\varphi}^{(k')} + \cdots + \mathcal{H}^{(k'+1)}\boldsymbol{\varphi}^{(0)}\right)\\ &\quad = \frac{\mathrm{i}}{2}\lambda_{k/2}^2\sigma\boldsymbol{\varphi}^{(0)}.\end{aligned} \tag{3.16}$$

By using the projection operator $\mathcal{P}$, we establish the equivalence between non-zero small eigenvalues of the operator $\sigma\mathcal{H}$ and non-zero eigenvalues of the reduced eigenvalue problems in the following theorem.

Theorem 3 (*Spectral Stability*). *Let Algorithm 1 converge at the K-th order and the solution $\boldsymbol{\phi}$ in Theorem 1 persist for $\epsilon \neq 0$. Let operator $\mathcal{H}$ have a small eigenvalue μ of multiplicity d, such that $\mu = \epsilon^k\mu_k + O(\epsilon^{k+1})$. Then, the eigenvalue problem (3.3) admits $(2d)$ small eigenvalues λ, such that $\lambda = \epsilon^{k/2}\lambda_{k/2} + O(\epsilon^{k/2+1})$, where non-zero values $\lambda_{k/2}$ are found from the quadratic eigenvalue problems*

$$\textit{odd } k: \quad \mathcal{M}^{(k)}\boldsymbol{\alpha} = \frac{1}{2}\lambda_{k/2}^2\boldsymbol{\alpha}, \tag{3.17}$$

$$\textit{even } k: \quad \mathcal{M}^{(k)}\boldsymbol{\alpha} + \frac{1}{2}\lambda_{k/2}\mathcal{L}^{(k)}\boldsymbol{\alpha} = \frac{1}{2}\lambda_{k/2}^2\boldsymbol{\alpha}, \tag{3.18}$$

$$\textit{where } \mathcal{L}^{(k)} = \mathcal{P}\left[\mathcal{H}^{(1)}\boldsymbol{\Phi}^{(k')}(\boldsymbol{\theta}_0) + \cdots + \mathcal{H}^{(k'+1)}\boldsymbol{\Phi}^{(0)}(\boldsymbol{\theta}_0)\right].$$

We note that matrix $\mathcal{L}^{(k)}$ must be skew-symmetrical so that all eigenvalues of the quadratic eigenvalue problem (3.18) occur in pairs $\lambda_{k/2}$ and $-\lambda_{k/2}$. This symmetry is standard for linearized Hamiltonian systems. Computations of small eigenvalues of the stability problem (3.3) can be achieved with a simple algorithm.

Algorithm 2 (*Spectral Stability*). Suppose that the solution $\boldsymbol{\phi}$ persists in Algorithm 1 and compute $\mathcal{M}^{(k)} = D_{\boldsymbol{\theta}}\mathbf{g}^{(k)}(\boldsymbol{\theta}_0)$ for $\kappa \leq k \leq K$.

1. For each order k, where eigenvalues of $\mathcal{M}^{(k)}$ are non-zero, compute matrices $\mathcal{L}^{(k)}$.
2. Find roots $\lambda_{k/2}$ of the determinant equation for the quadratic eigenvalue problems (3.17) and (3.18).

Example 1. Consider vortex configurations (2.9) on the simple cube (2.8). By explicit computations, the bifurcation equations are non-empty at the order $\kappa = 1$ and

$$\begin{aligned}g_{l,j}^{(1)} &= \sin(\theta_{l,j+1} - \theta_{l,j}) + \sin(\theta_{l,j-1} - \theta_{l,j})\\ &\quad + \sin(\theta_{l+1,j} - \theta_{l,j}), \quad l = 0, 1, \ j = 1, 2, 3, 4,\end{aligned} \tag{3.19}$$

where $\theta_{2,j} = \theta_{0,j}$. Roots of $\mathbf{g}^{(1)}(\boldsymbol{\theta})$ occur for vortex configurations (2.9) with $\theta_0 = \{0, \pi\}$ and $s_0 = \{+1, -1\}$. The other vortex configurations (2.9) with $\theta_0 = \{\frac{\pi}{2}, \frac{3\pi}{2}\}$ and $s_0 = \{+1, -1\}$ terminate at $k = 1$ of Algorithm 1. The Jacobian matrix $\mathcal{M}^{(1)}$ has eigenvalue $\lambda_{\neq 0}(\mathcal{M}^{(1)}) = 2$ of multiplicity 4 for $\theta_0 = 0$ and $s_0 = 1$, eigenvalue $\lambda_{\neq 0}(\mathcal{M}^{(1)}) = -2$ of multiplicity 4 for $\theta_0 = \pi$ and $s_0 = 1$, and two eigenvalues $\lambda_{\neq 0}(\mathcal{M}^{(1)}) = \{-2, 2\}$ of multiplicity 2 for $\theta_0 = 0$ and $s_0 = -1$. (The same result holds for $\theta_0 = \pi$ and $s_0 = -1$ by symmetry.) Algorithm 1 does not converge at $k = 1$, since $\mathrm{Ker}(\mathcal{M}^{(1)})$ is four-dimensional in all cases. Our symbolic computational results described in Example 2 indicate that Algorithm 1 converges at the order $K = 6$ and the vortex configurations above are uniquely continued in $\epsilon \in O(0)$ modulo the gauge transformation (3.9).

4. Computations of vortex configurations

We have created the symbolic package that performs all steps of Algorithms 1 and 2 described in Section 3. The user is supposed to input the configuration of active nodes S and the corresponding set of angles $\{\theta_n\}_{n\in S}$. The package performs computations order by order to detect if the phase configuration persists in the Lyapunov–Schmidt reduction algorithm and if it is spectrally stable. For all configurations (i)–(iii) described in Section 2, we have found that Algorithm 1 terminates at the finite order $k = K < \infty$ and the persistent configurations have $\boldsymbol{\theta}_* = \boldsymbol{\theta}_0$ up to the order $k = K$, where $\boldsymbol{\theta}_0$ is the root of the first non-empty correction $\mathbf{g}^{(\kappa)}(\boldsymbol{\theta})$ with $\kappa \geq 1$.

The package consists of two parts. The first part performs computations of the correction terms $\mathbf{g}^{(k)}(\boldsymbol{\theta}_0)$ of the vector field $\mathbf{g}(\boldsymbol{\theta}, \epsilon)$ and the Jacobian matrices $\mathcal{M}^{(k)} = D_{\boldsymbol{\theta}}\mathbf{g}^{(k)}(\boldsymbol{\theta}_0)$ for a given vector $\boldsymbol{\theta}_0$ with $\kappa \leq k \leq K$ according to Algorithm 1. We have confirmed that there exists $K < \infty$ such that $\dim\mathrm{Ker}(\mathcal{M}^{(K)}) = 1$. We have also checked that $\mathbf{g}^{(k)}(\boldsymbol{\theta}_0) \equiv 0$, $\kappa \leq k \leq K$ for all persistent configurations, such that no extension of the series (3.11) is necessary. All non-persistent configurations terminate because $\mathbf{g}^{(\kappa)}(\boldsymbol{\theta}_0) \neq 0$, i.e. the given vortex configuration $\boldsymbol{\theta}_0$ is not a root of the first non-empty correction $\mathbf{g}^{(\kappa)}(\boldsymbol{\theta})$.

Non-zero eigenvalues of $\mathcal{M}^{(k)}$ are recorded in the first part of the package for $\kappa \leq k \leq K$. By Theorem 2, these non-zero eigenvalues give approximations of the small eigenvalues of the linearized Hamiltonian $\mathcal{H}$ at the order of $O(\epsilon^k)$. The second part of the package performs computations of eigenvalues of the quadratic eigenvalue problems (3.17) and (3.18) according to Algorithm 2. Finding roots of the relevant determinant equations is not computationally difficult because the quadratic problem (3.17) is diagonal in λ^2 and the quadratic problem (3.18) is given typically by a matrix of small size.

Example 2. Continuing Example 1, we have found four non-zero eigenvalues of $\mathcal{M}^{(1)}$ at each persistent configuration, which result in four pairs of small eigenvalues $\lambda_{1/2}$ of the quadratic problem (3.17). For instance, since the vortex configuration (2.9) with $\theta_0 = \pi$ and $s_0 = 1$ has $\lambda_{\neq 0}(\mathcal{M}^{(1)}) = -2$ of multiplicity 4, the quadratic problem (3.17) has a pair of eigenvalues $\lambda_{1/2} = \pm\sqrt{2\lambda_{\neq 0}(\mathcal{M}^{(1)})} = \pm 2\mathrm{i}$ of multiplicity 4. Continuing Algorithms 1 and 2 to the order $k = 2$, we find two non-zero eigenvalues of $P^{(1)}\mathcal{M}^{(2)}P^{(1)}$ for each

Table 1
Vortex configurations (2.9) on the simple cube (2.8)

S_1	Persists	Eigenvalues of $\mathcal{H}$			Eigenvalues of $i\sigma\mathcal{H}$			Stable
		ϵ	ϵ^2	ϵ^6	$\epsilon^{1/2}$	ϵ	ϵ^3	
$\{0, \frac{\pi}{2}, \pi, \frac{3\pi}{2}\}$	Yes	$\{2 \times 4\}$	$\{2 \times 2\}$	$\{-16\}$	$\{\pm 2 \times 4\}$	$\{\pm 2i \times 2\}$	$\{\pm 4i\sqrt{2}\}$	No
$\{0, \frac{3\pi}{2}, \pi, \frac{\pi}{2}\}$	Yes	$\{-2 \times 2, 2 \times 2\}$	$\{2 \times 2\}$	$\{-16\}$	$\{\pm 2 \times 2, \pm 2i \times 2\}$	$\{\pm 2 \times 2\}$	$\{\pm 4i\sqrt{2}\}$	No
$\{\frac{\pi}{2}, \pi, \frac{3\pi}{2}, 0\}$	No							
$\{\frac{\pi}{2}, 0, \frac{3\pi}{2}, \pi\}$	No							
$\{\pi, \frac{3\pi}{2}, 0, \frac{\pi}{2}\}$	Yes	$\{-2 \times 4\}$	$\{2 \times 2\}$	$\{-16\}$	$\{\pm 2i \times 4\}$	$\{\pm 2i \times 2\}$	$\{\pm 4i\sqrt{2}\}$	Yes
$\{\frac{3\pi}{2}, 0, \frac{\pi}{2}, \pi\}$	No							

Table 2
Vortex configurations (2.11) on the double cross (2.10)

S_1	Persists	Eigenvalues of $\mathcal{H}$		Eigenvalues of $i\sigma\mathcal{H}$		Stable
		ϵ^2	ϵ^4	ϵ	ϵ^2	
$\{0, \frac{\pi}{2}, \pi, \frac{3\pi}{2}\}$	Yes	$\{-2 \times 2, 2 \times 2\}$	$\{-8, 28 \times 2\}$	$\{\pm 2 \times 2, \pm 2i \times 2\}$	$\{\pm 4i, \pm 2\sqrt{14} \times 2\}$	No
$\{0, \frac{3\pi}{2}, \pi, \frac{\pi}{2}\}$	Yes	$\{-4, -2 \times 3, 2\}$	$\{-8, 28\}$	$\{\pm 2, \pm 2i \times 3, \pm 2i\sqrt{2}\}$	$\{\pm 4i, \pm 2\sqrt{14}\}$	No
$\{\frac{\pi}{2}, \pi, \frac{3\pi}{2}, 0\}$	No					
$\{\frac{\pi}{2}, 0, \frac{3\pi}{2}, \pi\}$	No					
$\{\pi, \frac{3\pi}{2}, 0, \frac{\pi}{2}\}$	Yes	$\{-4 \times 2, -2 \times 4\}$	$\{-8\}$	$\{\pm 2i \times 4, \pm 2i\sqrt{2} \times 2\}$	$\{\pm 4i\}$	Yes
$\{\frac{3\pi}{2}, 0, \frac{\pi}{2}, \pi\}$	No					

Table 3
Configurations (2.13) on the diamond (2.12)

S_{-1}	S_1	Persists	Eigenvalues of $\mathcal{H}$		Eigenvalues of $i\sigma\mathcal{H}$		Stable
			ϵ^2	ϵ^4	ϵ	ϵ^2	
0	0	Yes	$\{-12, -6, 2 \times 2, 4\}$		$\{\pm 2 \times 2, \pm 2\sqrt{2}, \pm 2i\sqrt{3}, \pm 2i\sqrt{6}\}$		No
0	$\frac{\pi}{2}$	No					
0	π	Yes	$\{-2 \times 2, -5 \pm \sqrt{41}\}$	12	$\{\pm 2i \times 2, \pm\sqrt{-10 + 2\sqrt{41}}, \pm i\sqrt{10 + 2\sqrt{41}}\}$	$\pm 2\sqrt{6}$	No
$\frac{\pi}{2}$	$\frac{\pi}{2}$	No					
$\frac{\pi}{2}$	π	No					
$\frac{\pi}{2}$	$\frac{3\pi}{2}$	Yes	$\{-8, -2 \times 3\}$	-12	$\{\pm 2i \times 3, \pm 4i\}$	$\pm 2i\sqrt{6}$	Yes

configuration, which result in two pairs of small eigenvalues λ_1 of the quadratic problem (3.18) with a non-zero matrix $\mathcal{L}^{(2)}$. For the same selected configuration, $\lambda_{\neq 0}(P^{(1)}\mathcal{M}^{(2)}P^{(1)}) = 2$ of multiplicity 2, whereas the quadratic problem (3.18) has a pair of eigenvalues $\lambda_1 = \pm 2i$ of multiplicity 2. Continuing the algorithm, we have found no non-zero eigenvalues for matrices $P^{(2)}\mathcal{M}^{(3,4,5)}P^{(2)}$ and the last non-zero eigenvalue for the matrix $P^{(2)}\mathcal{M}^{(6)}P^{(2)}$ for each vortex configuration, such that $K = 6$. The non-zero eigenvalue of $P^{(2)}\mathcal{M}^{(6)}P^{(2)}$ results in a pair of small eigenvalues λ_3 of the quadratic problem (3.18), where the matrix $\mathcal{L}^{(6)}$ was found to be identically zero in each case. For the same selected configuration, the last non-zero eigenvalue is $\lambda_{\neq 0}(P^{(2)}\mathcal{M}^{(6)}P^{(2)}) = -16$ and a pair of simple eigenvalues of the quadratic problem (3.18) is $\lambda_3 = \pm\sqrt{2\lambda_{\neq 0}(P^{(2)}\mathcal{M}^{(6)}P^{(2)})} = \pm 4\sqrt{2}i$. The output of the Mathematica symbolic computational package for the selected vortex configuration is attached to the electronic version of this article.

Similar to Example 2, we have performed computations of all configurations (i)–(iii) listed in Section 2. Our results are summarized in Tables 1–3 where we list the conclusions of Algorithms 1 and 2, the orders for non-zero small eigenvalues of $\mathcal{H}$ and $i\sigma\mathcal{H}$, and the leading-order approximations of eigenvalues in accordance to the following convention: the entry 2×4 on the first line of Table 1 denotes the non-zero eigenvalue 2 of algebraic multiplicity 4 for a persistent vortex configuration.

5. Comparison with full eigenvalue computations

We proceed to test the predictions of the symbolic computations against the results of direct numerical approximations of relevant configurations and associated eigenvalues. Starting from the anti-continuum limit where the solutions (2.7) are explicit, we use numerical continuation techniques to obtain the corresponding solutions of the difference equations (2.4) for finite coupling strengths of $\epsilon < 0.2$. Numerical approximations of the vortex solutions are obtained with the fixed point iterations using Newton's method. Examples of the output of the fixed point iterations for representative members of each of the families (vortex cube, double cross and diamond) are shown

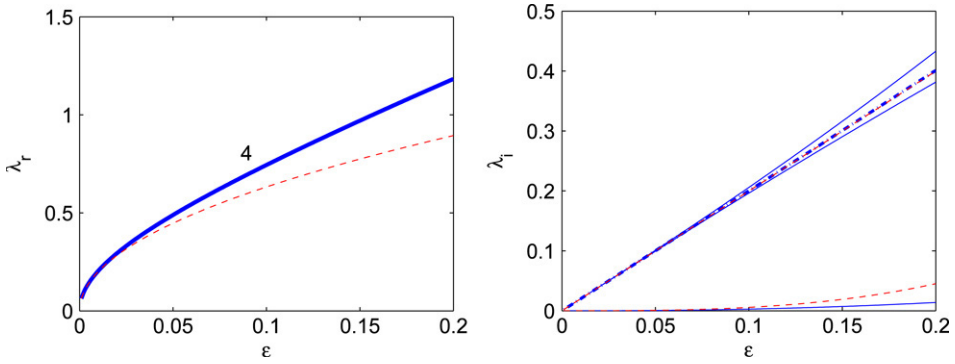

Fig. 2. The real (left) and imaginary (right) parts of small eigenvalues of the linearized problem (2.6) associated with the vortex cube configuration with $S_1 = \{0, \frac{\pi}{2}, \pi, \frac{3\pi}{2}\}$ versus ϵ. Numerically computed eigenvalues are denoted by solid (blue in the web version) lines, while their counterparts from symbolic computations are plotted by dashed (red in the web version) lines. Multiple real or imaginary eigenvalues are denoted by thick solid lines and their corresponding multiplicity is shown beside the relevant line, while complex eigenvalues are denoted by thick dash-dotted lines.

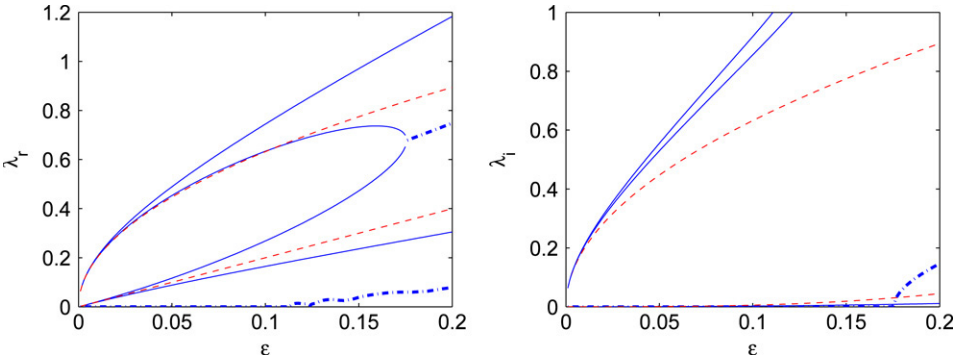

Fig. 3. Same as in Fig. 2, but for the simple cube vortex configuration with $S_1 = \{0, \frac{3\pi}{2}, \pi, \frac{\pi}{2}\}$.

in Fig. 1 for $\epsilon = 0.1$. Once the solution $\{\phi_n\}_{n\in\mathbb{Z}^3}$ is obtained to the desired numerical accuracy (typically 10^{-8}) on a truncated numerical domain, the eigenvalue problem (2.6) becomes a large matrix eigenvalue problem, which is fully solved using standard numerical algebra tools. The relevant eigenvalues with small real and imaginary parts are isolated and their dependence on ϵ is accordingly extracted and compared to the theoretical predictions of Tables 1–3. The results are shown in Figs. 2–10, which are discussed in more detail below. In general, we denote numerically computed eigenvalues by solid (blue in the web version) lines, while their counterparts from symbolic computations are plotted by dashed (red in the web version) lines. Pairs of multiple real or imaginary eigenvalues are denoted by thick solid lines, while quartets of complex eigenvalues are denoted by thick dash-dotted lines. In all the cases of thick solid lines, the multiplicity of the relevant numerical eigenvalues is also shown beside the corresponding line. In all the cases of complex quartets that arise here, there is a single quartet involved (e.g. there are no cases with multiple identical complex quartets).

Fig. 2 corresponds to the simple cube configuration with $S_1 = \{0, \frac{\pi}{2}, \pi, \frac{3\pi}{2}\}$. As is indicated in Table 1, this configuration should be unstable due to an eigenvalue $\lambda \approx 2\epsilon^{1/2}$, of multiplicity four. What we find, however, is that the pair of quadruple real eigenvalue splits in a pair of double real eigenvalues and a quartet of complex eigenvalues. To make things even more interesting, all four eigenvalues in the right-

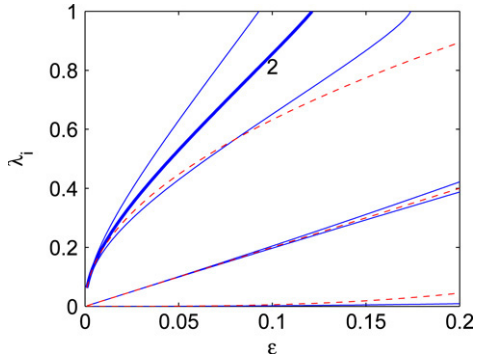

Fig. 4. Same as in Fig. 2, but for the stable simple cube vortex configuration with $S_1 = \{\pi, \frac{3\pi}{2}, 0, \frac{\pi}{2}\}$.

half plane have the same real part denoted by the very thick solid line in the left panel of Fig. 2. The imaginary part of the quartet of complex eigenvalues is denoted by a dash-dotted line in the right panel of the figure. If the real part of all four eigenvalues is at the order $O(\epsilon^{1/2})$, the imaginary part of complex eigenvalues occurs at the order $O(\epsilon)$ with a numerical approximation $\lambda \approx 2\epsilon^{1/2} \pm 2i\epsilon$. Besides these four eigenvalues in the right-half plane, Table 1 also reports existence of a pair of double imaginary eigenvalues at the order $O(\epsilon)$ and a pair of simple, imaginary eigenvalues at the order $O(\epsilon^3)$. All these eigenvalues are shown on the right panel of Fig. 2 by thin lines, since the pair of double imaginary eigenvalues splits into two pairs of simple imaginary eigenvalues. We can see that,

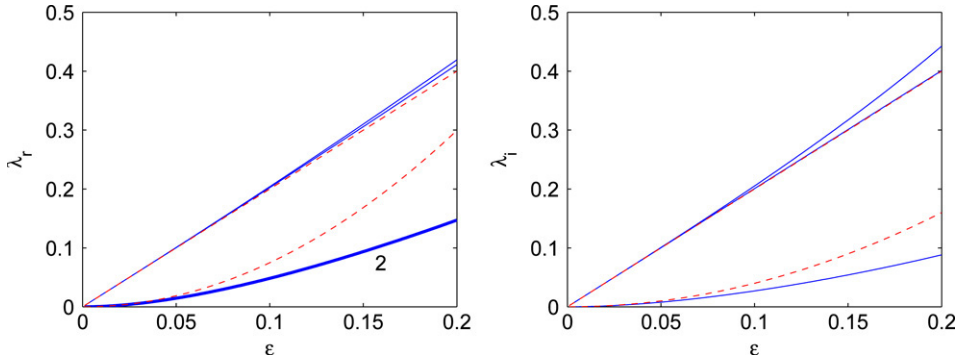

Fig. 5. Same as Fig. 2, but for the double-cross vortex configuration with $S_1 = \{0, \frac{\pi}{2}, \pi, \frac{3\pi}{2}\}$.

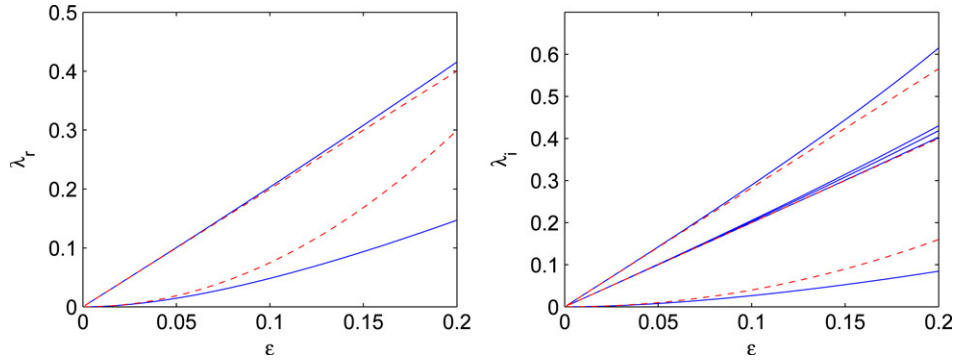

Fig. 6. Same as Fig. 2, but for the double-cross vortex configuration with $S_1 = \{0, \frac{3\pi}{2}, \pi, \frac{\pi}{2}\}$.

although the results of Table 1 give only the leading-order approximations of small eigenvalues of the linearized problem, they represent adequately the pattern of unstable and neutrally stable eigenvalues.

Fig. 3 describes another simple cube vortex configuration of Table 1 with $S_1 = \{0, \frac{3\pi}{2}, \pi, \frac{\pi}{2}\}$. As theoretically predicted, we find this configuration to be immediately unstable, due to a double pair of real eigenvalues at the order $O(\epsilon^{1/2})$ and another double pair of real eigenvalues of the order $O(\epsilon)$. Both pairs split for small values of ϵ but remain simple pairs of real eigenvalues for sufficiently small values of ϵ. Then, a pair of the former and one of the latter collide for $\epsilon \approx 0.175$, leading to a quartet of complex eigenvalues. Another double pair of imaginary eigenvalues exists at the order $O(\epsilon^{1/2})$ and it splits into simple pairs of imaginary eigenvalues. When these eigenvalues meet the continuous spectrum located at $\pm i[1, 1 + 6\epsilon]$, the pairs of imaginary eigenvalues generate additional quartets of complex eigenvalues for $\epsilon > 0.113$ and $\epsilon > 0.125$. Finally, one more pair of imaginary eigenvalues exists at the order $O(\epsilon^3)$ and it remains small for $0 < \epsilon < 0.2$.

Fig. 4 describes the third simple cube vortex configuration of Table 1 with $S_1 = \{\pi, \frac{3\pi}{2}, 0, \frac{\pi}{2}\}$, which is spectrally stable for small ϵ. The quadruple pair of imaginary eigenvalues at the order $O(\epsilon^{1/2})$ splits for small ϵ into a double pair and two simple pairs of imaginary eigenvalues. All these pairs generate quartets of complex eigenvalues upon collision with the continuous spectrum for $\epsilon > 0.1$, $\epsilon > 0.125$ and $\epsilon > 0.174$. Therefore, the vortex configuration becomes unstable for sufficiently large ϵ. A double pair of imaginary eigenvalues at the order $O(\epsilon)$ splits for small ϵ into simple pairs of imaginary

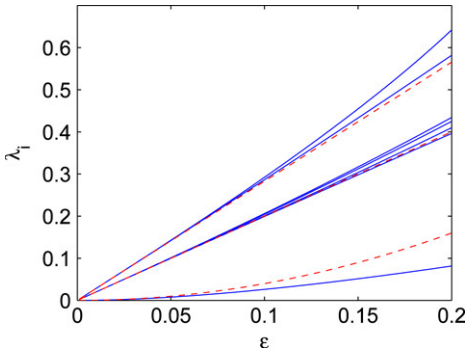

Fig. 7. Same as Fig. 2, but for the stable double-cross vortex configuration with $S_1 = \{\pi, \frac{3\pi}{2}, 0, \frac{\pi}{2}\}$.

eigenvalues. The additional pair of imaginary eigenvalues at the order $O(\epsilon^3)$ remains small for $0 < \epsilon < 0.2$.

The double-cross vortex configuration of Table 2 with $S_1 = \{0, \frac{\pi}{2}, \pi, \frac{3\pi}{2}\}$ is shown in Fig. 5. The results are fully consistent with the leading-order approximations of eigenvalues. We note, however, that both double pairs of real and imaginary eigenvalues at the order $O(\epsilon)$ split for small ϵ into simple pairs of real and imaginary eigenvalues, while the double pair of real eigenvalues at the order $O(\epsilon^2)$ remains double for small ϵ.

The double-cross vortex configuration of Table 2 with $S_1 = \{0, \frac{3\pi}{2}, \pi, \frac{\pi}{2}\}$ is shown in Fig. 6. All pairs of real and imaginary eigenvalues are simple including the triple pair of imaginary eigenvalues at the order $O(\epsilon)$ which splits for small ϵ into three simple pairs of imaginary eigenvalues.

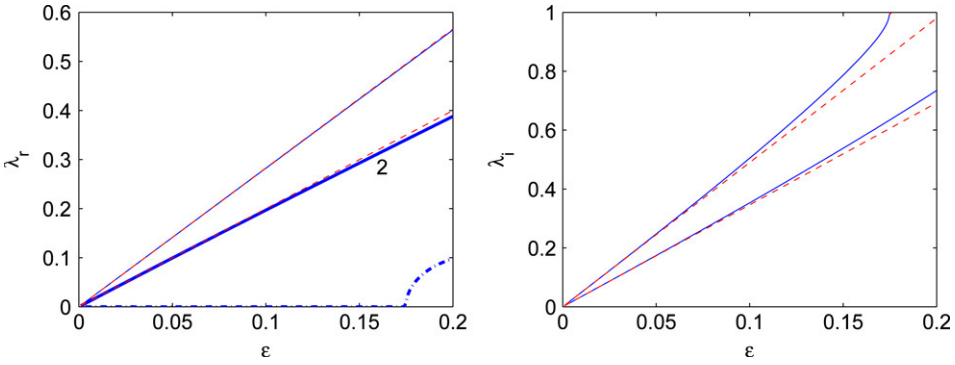

Fig. 8. The real and imaginary parts of the pertinent eigenvalues of the diamond configuration with $S_{-1} = 0$ and $S_1 = 0$ as a function of ϵ.

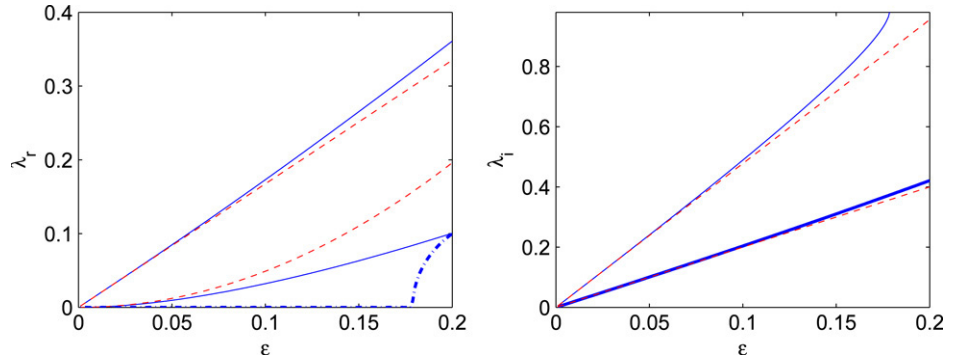

Fig. 9. Same as in Fig. 8, but for the diamond configuration with $S_{-1} = 0$ and $S_1 = \pi$.

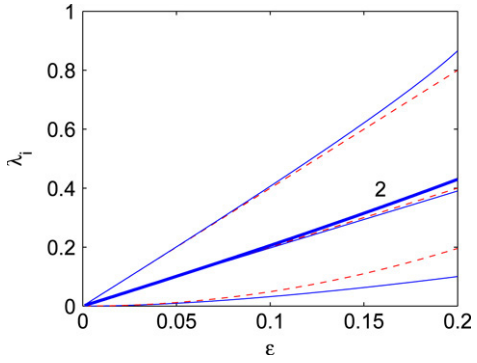

Fig. 10. Same as in Fig. 8, but for the stable diamond vortex configuration with $S_{-1} = \frac{\pi}{2}$ and $S_1 = \frac{3\pi}{2}$.

Finally, the double-cross vortex configuration of Table 2 with $S_1 = \{\pi, \frac{3\pi}{2}, 0, \frac{\pi}{2}\}$ is found to be spectrally stable for $\epsilon < 0.2$ and is shown in Fig. 7. The double and quadruple pairs of imaginary eigenvalues at the order $O(\epsilon)$ split for small ϵ into individual simple pairs of imaginary eigenvalues. We note that the domain of stability of this vortex cross configuration is wider than the one for the simple cube vortex configuration on Fig. 4, since no bifurcation of complex eigenvalues occur up to $\epsilon = 0.2$.

Lastly, we turn to the diamond configurations of Table 3. For the case of $S_{-1} = 0$ and $S_1 = 0$, shown in Fig. 8, the configuration is unstable due to a simple and a double pair of real eigenvalues, both of $O(\epsilon)$, captured very accurately by our theoretical approximation. In addition, a complex quartet emerges because of the collision of a pair of imaginary eigenvalues with the continuous spectrum for $\epsilon > 0.175$.

The second diamond configuration with $S_{-1} = 0$ and $S_1 = \pi$, shown in Fig. 9, is unstable due to two simple pairs of real eigenvalues, one at the order $O(\epsilon)$ and one at the order $O(\epsilon^2)$. The simple pair of imaginary eigenvalues becomes a quartet of complex eigenvalues upon collision with the continuous spectrum for $\epsilon > 0.179$. The double pair of imaginary eigenvalues remains double for $0 < \epsilon < 0.2$.

Finally, the third diamond vortex configuration with $S_{-1} = \frac{\pi}{2}$ and $S_1 = \frac{3\pi}{2}$, shown in Fig. 10, is spectrally stable for $0 < \epsilon < 0.2$. In this case also, the theoretical prediction accurately captures the simple pair of imaginary eigenvalues at the order $O(\epsilon)$, the triple pair of imaginary eigenvalues (splitting into a double pair and a simple one) at the order $O(\epsilon)$, and the simple pair of imaginary eigenvalues at the order $O(\epsilon^2)$.

6. Conclusion

The main benefit of the present paper is that it provides a systematic computational approach, based on a symbolic mathematical package to unravel the existence and linear stability of any configuration of interest in a three-dimensional lattice that is of paramount interest in a wide range of applications. The package implements the conditions of the Lyapunov–Schmidt reduction method that are necessary and, in the case of convergence, sufficient for persistence of relevant configurations from the anti-continuum limit of the lattice. The algorithm subsequently connects the leading-order behaviour of

the small eigenvalues of the stability problem (which bifurcate from the zero eigenvalue and are responsible for the instability of the vortex configurations) to the Jacobian matrix of the above conditions. In so doing, it provides a powerful predictor that we have always found to be accurate for small values of the coupling parameter. We thus believe that this work provides a valuable tool that can be used to examine various configurations that may be of interest to both theoretical and experimental studies in optical and soft condensed-matter systems.

Acknowledgements

M.L. is supported by the NSERC USRA scholarship. D.P. is supported by the NSERC Discovery grant and the EPSRC Research Fellowship. P.G.K. is supported by NSF through the grants DMS-0204585, DMS-CAREER, DMS-0505663 and DMS-0619492.

References

[1] D.N. Christodoulides, F. Lederer, Y. Silberberg, Nature 424 (2003) 817–823.
[2] J.W. Fleischer, G. Bartal, O. Cohen, T. Schwartz, O. Manela, B. Freeman, M. Segev, H. Buljan, N.K. Efremidis, Opt. Express 13 (2005) 1780–1796.
[3] V.V. Konotop, V.A. Brazhnyi, Modern Phys. Lett. B 18 (2004) 627–651;
O. Morsch, M. Oberthaler, Rev. Modern Phys. 78 (2006) 179–215;
P.G. Kevrekidis, D.J. Frantzeskakis, Modern Phys. Lett. B 18 (2004) 173–202.
[4] P. Binder, D. Abraimov, A.V. Ustinov, S. Flach, Y. Zolotaryuk, Phys. Rev. Lett. 84 (2000) 745–748;
E. Trías, J.J. Mazo, T.P. Orlando, Phys. Rev. Lett. 84 (2000) 741–744.
[5] M. Sato, B.E. Hubbard, A.J. Sievers, Rev. Modern Phys. 78 (2006) 137–157.
[6] M. Peyrard, Nonlinearity 17 (2004) R1–R40.
[7] S. Aubry, Physica D 103 (1997) 201–250;
S. Flach, C.R. Willis, Phys. Rep. 295 (1998) 181–264;
D. Hennig, G. Tsironis, Phys. Rep. 307 (1999) 333–432.
[8] P.G. Kevrekidis, K.Ø. Rasmussen, A.R. Bishop, Int. J. Modern Phys. B 15 (2001) 2833–2900;
J.C. Eilbeck, M. Johansson, in: L. Vazquez, et al. (Eds.), Proceedings of the 3rd Conference on Localization and Energy Transfer in Nonlinear Systems, World Scientific, New Jersey, 2003, pp. 44–67.
[9] C. Sulem, P.L. Sulem, The Nonlinear Schrödinger Equation, Springer-Verlag, New York, 1999.
[10] D.N. Christodoulides, R.I. Joseph, Opt. Lett. 13 (1988) 794–796.
[11] G.L. Alfimov, P.G. Kevrekidis, V.V. Konotop, M. Salerno, Phys. Rev. E 66 (2002) 046608;
N.K. Efremidis, D.N. Christodoulides, Phys. Rev. A 67 (2003) 063608.
[12] H.S. Eisenberg, Y. Silberberg, R. Morandotti, A.R. Boyd, J.S. Aitchison, Phys. Rev. Lett. 81 (1998) 3383–3386.
[13] R. Morandotti, U. Peschel, J.S. Aitchison, H.S. Eisenberg, Y. Silberberg, Phys. Rev. Lett. 83 (1999) 2726–2729.
[14] J. Meier, G.I. Stegeman, D.N. Christodoulides, Y. Silberberg, R. Morandotti, H. Yang, G. Salamo, M. Sorel, J.S. Aitchison, Phys. Rev. Lett. 92 (2004) 163902.
[15] A. Smerzi, A. Trombettoni, P.G. Kevrekidis, A.R. Bishop, Phys. Rev. Lett. 89 (2002) 170402;
F.S. Cataliotti, L. Fallani, F. Ferlaino, C. Fort, P. Maddaloni, M. Inguscio, New J. Phys. 5 (2003) 71.
[16] D.N. Neshev, T.J. Alexander, E.A. Ostrovskaya, Yu.S. Kivshar, H. Martin, I. Makasyuk, Z. Chen, Phys. Rev. Lett. 92 (2004) 123903;
J.W. Fleischer, G. Bartal, O. Cohen, O. Manela, M. Segev, J. Hudock, D.N. Christodoulides, Phys. Rev. Lett. 92 (2004) 123904.
[17] D.E. Pelinovsky, P.G. Kevrekidis, D.J. Frantzeskakis, Physica D 212 (2005) 1–19.
[18] D.E. Pelinovsky, P.G. Kevrekidis, D. Frantzeskakis, Physica D 212 (2005) 20–53;
P.G. Kevrekidis, D.E. Pelinovsky, Proc. R. Soc. A 462 (2006) 2671–2694.
[19] P.G. Kevrekidis, B.A. Malomed, D.J. Frantzeskakis, R. Carretero-González, Phys. Rev. Lett. 93 (2004) 080403;
R. Carretero-González, P.G. Kevrekidis, B.A. Malomed, D.J. Frantzeskakis, Phys. Rev. Lett. 94 (2005) 203901.
[20] J.E. Heebner, R.W. Boyd, J. Modern Opt. 49 (2002) 2629–2636;
P. Chak, J.E. Sipe, S. Pereira, Opt. Lett. 28 (2003) 1966–1968.